This is the author's version of an article that has been published in this journal. Changes were made to this version by the publisher prior to publication.
The final version of record is available at http://dx.doi.org/10.1109/TPEL.2016.2610323

A High Efficiency Helical Core for Magnetic Field Energy Harvesting

Sheng Yuan, Yi Huang, *Senior Member, IEEE*, Jiafeng Zhou, Qian Xu, Chaoyun Song and Guoqiang Yuan

***Abstract*—Real-time data of high voltage infrastructures collected by wireless sensors are the foundation of many smart grid applications. Energy harvesting can be an effective solution for autonomous, self-powered wireless sensors. In this paper, a coil with a novel helical core is proposed and optimized to scavenge the magnetic field energy efficiently near equipment carrying large currents. Due to the special design of the helical core, the path of the magnetic flux inside the core can be significantly increased, which leads to a reduction of the demagnetizing field. Therefore, the proposed core can generate a much higher flux density (hence more power) compared with conventional designs. The selection of the core material is studied and it is found that high permeability ferrite is the most suitable material. Experimental results show that the proposed helical coil with only 400 turns of wire can have a power density of 2.1 μW/cm^3 when placed in a magnetic flux density of 7 μT$_{rms}$. This value is bigger than any of the existing designs if placed in the same magnetic field. If more wires can be wound on the core, an even higher power density could be obtained. Therefore, the proposed design is a very efficient method for scavenging the magnetic field energy for a wide range of smart grid applications.**

***Index Terms*— Energy harvesting, inductive coil, magnetic field, smart grid.**

I. INTRODUCTION

Due to global urbanization and the rapid development of mega cities, it is expected that the demand for electric energy will continue to increase in the coming decades [1]. It is a big challenge to deliver this huge energy from power plants to end customers, as the existing power distribution systems may reach to their thermal limitations [2]. Furthermore, the increasing load on high voltage equipment could accelerate the deterioration of the insulation [3]. For old equipment, it is more likely to breakdown due the aging effect and the heavy load. To deal with these problems and pressures, several smart grid technologies (such as dynamic thermal rating [4], demand response [5] and real-time condition monitoring [6]) are being developed. It is important to note that smart grid technologies have relied heavily on the real-time data (e.g. current, voltage and temperature) from high power equipment such as transformers, switchgears, overhead lines, etc. Wireless sensors are considered to be favorable tools for collecting these data because of their low power consumption, rapid deployment and low cost [7]. However, the finite life span of the batteries which power the sensing system is a bottleneck as it is expensive to replace these batteries periodically. Thus, the energy harvesting technology is an attractive solution to make wireless sensors self-sustainable [8].

There are several ambient energy sources (solar, wind, electrical field, magnetic field, etc.) in electrical substations or under electricity pylons. As discussed in our previous work [9], the magnetic field energy is a suitable energy source near any equipment that carries sufficient currents, because it is reliable and relatively easy to collect. There are two types of magnetic field energy harvesters working for different purposes.

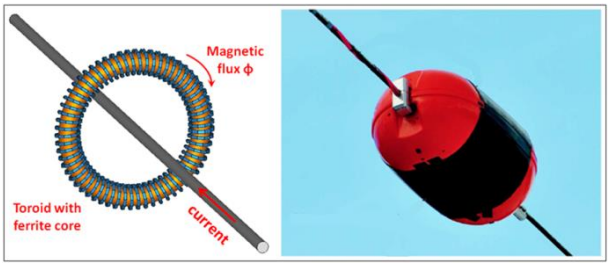

Fig. 1. Energy harvesters mounted on a power line.

The first type is the cable-clamped energy harvester [10-13]. A toroid is mounted on a power cable as shown in Fig. 1 [14]. As the coil can fully enclose the current conductor, the power density of this type of energy harvester is relatively high. It is mainly used to power the sensors which measure the line current and the cable temperature.

The second type is the free-standing energy harvester as shown in Fig. 2 [9]. Unlike the cable-clamped type, this energy harvester can be installed in any place as long as there is an

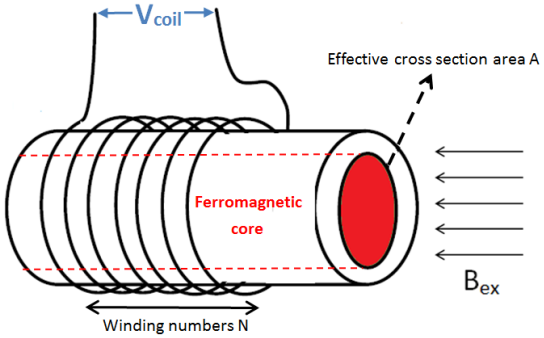

Fig. 2. A free-standing solenoid placed inside an alternating magnetic field

Manuscript received April 07, 2016; revised May 30, 2016; accepted August 24, 2016.

S. Yuan, Y. Huang, J. Zhou, Q. Xu and C. Song are with the University of Liverpool, Department of Electrical Engineering and Electronics, Liverpool, L69 3GJ, UK (Corresponding author, yi.huang@liv.ac.uk).

G. Yuan is with Shanghai CSY Ltd; No.18，Lane255, Luoyang Road, Shanghai, China.

Copyright (c) 2016 IEEE. Personal use is permitted. For any other purposes, permission must be obtained from the IEEE by emailing pubs-permissions@ieee.org.

This is the author's version of an article that has been published in this journal. Changes were made to this version by the publisher prior to publication.
The final version of record is available at http://dx.doi.org/10.1109/TPEL.2016.2610323

alternating magnetic field. Because of the great flexibility, the harvesting coil is capable of powering various sensors for different purposes. For example, partial discharge sensors can be powered to monitor the conditions of transformers in electrical substations. Weather stations placed under overhead lines can be powered by a free-standing energy harvester to collect the real-time weather data (such as wind speed, humidity, air temperature, etc.), which is the foundation of the dynamic thermal rating technique. Since the harvesting coil cannot fully enclose the current conductor, the demagnetization phenomenon, which will be discussed in Fig. 4, appears during the magnetization process, which decreases the effective permeability μ_{eff}. As a consequence, the power output is greatly limited compared to the cable-clamped coil [9, 15]. Tashiro *et al* used Brooks coils to harvest the energy from the power line [16]. From their experiments, a power density of 1.47 μW/cm^3 was achieved in an area with a magnetic flux density of 21.2 μT$_{rms}$ at 60 Hz. Their power density was limited due to the core shape and material. Roscoe *et al* suggested that a coil with a long and thin ferromagnetic core can increase the effective permeability and produce a higher power output. They designed a 50 cm long solenoid with a diameter of 5 cm to collect the magnetic field energy in a substation [15, 17]. The power density from their coil was 0.845 μW/cm^3 when it was placed in a magnetic flux density of 18.5 μT$_{rms}$ at 50 Hz. They selected cast iron as the core material which suffered greatly from the eddy current losses. Besides, their coil may be too long for some applications. Moghe *et al* proposed the idea of the flux concentrator to increase the magnetic flux density inside the ferromagnetic core [18-19]. An X-shaped core with 300 turns of wire and a length of 6 cm was developed and placed on a conductor carrying a current of 900 A. The power density of their coil was about 2.4 mW/cm^3 where the magnetic flux density is around 7 mT$_{rms}$. The power density is limited due to the small number of turns and the short length of the core. In our previous work [9], a bow-tie shaped coil was proposed which used the idea of flux concentration. The harvesting coil was studied and optimized in terms of the effective permeability, the core material selection and the winding method. The experiment results showed that the proposed bow-tie coil with a length of 15 cm could achieve a power density of 1.86 μW/cm^3 when placed in a magnetic flux density of 7 μT$_{rms}$ at 50 Hz. This value is 15 times greater than the results from [15] under the same testing conditions.

In this paper, a more efficient free-standing magnetic field energy harvester is proposed where the path of the magnetic flux in its new helical core can be lengthened dramatically so that the demagnetization factor is much reduced. Therefore, the magnetic flux density in the core can be significantly increased and more power can be collected. The design details of this energy harvester are presented in Section II. In Section III, the parameters of the helical core are studied. In Section IV, the experiment evaluations of the proposed design are presented. The discussions and conclusions are given in Section V and Section VI, respectively.

II. The Energy Harvester Design

A. System Modelling

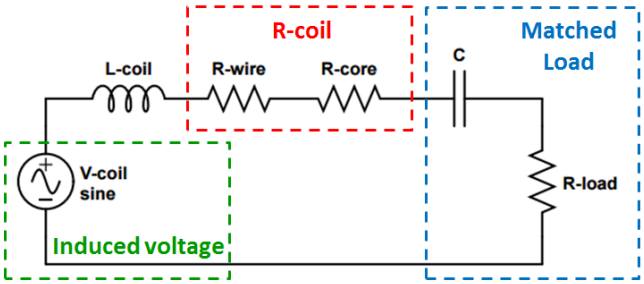

Fig. 3. The equivalent circuit of a harvesting coil with a matched load.

At 50/60 Hz, the most efficient way to harvest the magnetic energy is to employ coils wrapped typically on ferromagnetic cores. Although the coil is not directly clamped on a current conductor, the whole system is still an inductive coupling circuit. Fig. 3 shows the equivalent circuit of a harvesting coil connected with a matched load. The induced coil voltage V_{coil} is a function of the surrounding magnetic flux density and the coil properties by applying Faraday's Law as shown in Fig. 2 [9]:

$$V_{coil} = N\omega B_{ex} A \mu_{eff} \quad (1)$$

where V_{coil} is the RMS (root mean square) voltage of the AC waveform, N is the number of turns wound on the coil, B_{ex} is the external magnetic flux density in T$_{rms}$ applied to the coil, A represents the effective cross section area of the coil in m^2, ω is the angular frequency in rad/s and μ_{eff} is the effective permeability related to the core material and core geometry. From previous research summarized in Table I, the magnetic flux density of 7 μT$_{rms}$ is usually available under overhead lines or inside electric substations. In this paper, this value is used as the magnetic flux density in the software simulation as well as in the experiment.

TABLE I
THE SURVEY OF MAGNETIC FIELD NEAR HIGH POWER EQUIPMENT

Test environment	Test conditions	Magnetic flux density
400 kV L12 overhead lines	2 meters above the ground I_{rms} = 500 A	7 μT [9, 20]
132 kV L7 overhead lines	5 meters above the ground I_{rms} = 700 A	11.0 μT [20]
400 kV L12 overhead lines	3 meters above the ground I_{rms} = 700 A	11.3 μT [20]
11 kV indoor substation	Near high voltage transformers and switchgears	15 - 20 μT [21]
150 kV outdoor substation	Near high voltage transformers	26 - 28 μT [22]
345 kV outdoor substation	Close to high voltage circuit breakers	30 - 40 μT [23]

The effective coil resistance R_{coil} consists of two parts: wire resistance R_{wire} and equivalent core resistance R_{core}. The wire resistance is caused by the resistance of the long enameled wire wound on the core. The equivalent core resistance is due to the

Copyright (c) 2016 IEEE. Personal use is permitted. For any other purposes, permission must be obtained from the IEEE by emailing pubs-permissions@ieee.org.

This is the author's version of an article that has been published in this journal. Changes were made to this version by the publisher prior to publication.
The final version of record is available at http://dx.doi.org/10.1109/TPEL.2016.2610323

eddy current losses and hysteresis losses when the core is subject to a time-varying magnetic field.

It is important to have a matched load to ensure the maximum power transfer from the coil to the load. According to maximum power transfer theory, a compensating capacitor is added in series to eliminate the coil inductance L_{coil}. And the load resistance R_{load} should have the same value as the coil resistance. Under these conditions, *the power density* (the output power per unit volume, which is different from the definition of the power density in electromagnetics) of this harvesting coil can be derived to be [9]:

$$S_{power} = \frac{1}{4}\frac{{V_{coil}}^2}{R_{coil}}/Vol \quad (2)$$

where Vol is the total volume of the coil in m^3. To maximize the power output from the coil, its coil voltage V_{coil} should be increased while the coil resistance must be minimized. These two variables are correlated with the core shape, the core material and the properties of the enameled wires.

B. Optimum Core Shape Design

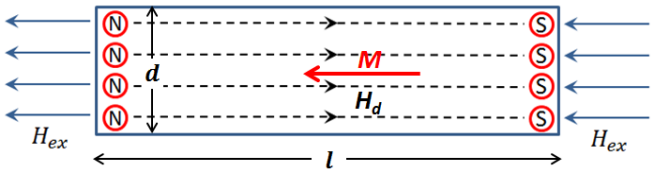

Fig. 4. The demagnetizing field H_d inside a ferromagnetic rod when applying an external magnetic field H_{ex}

It is noted that the effective permeability μ_{eff} is an important parameter which can affect the induced voltage and the power output significantly. It can be reduced dramatically due to the demagnetization phenomenon as shown in Fig. 4: when a ferromagnetic rod with a finite length is magnetized, the north and south poles are created at two opposite sides, leading to a demagnetizing field H_d. The demagnetizing field H_d depends on the magnetization M inside the core and the demagnetization factor D_M [24].

$$H_d = D_M \times M \quad (3)$$

D_M is solely determined by the core shape and the effective permeability μ_{eff} can be expressed:

$$\mu_{eff} = \frac{\mu_r}{1 + D_M(\mu_r - 1)} \quad (4)$$

where μ_r is the relative permeability of the core material. The core shape needs to be optimized to reduce the demagnetization factor and increase the effective permeability. The conventional method suggests that a thin and long rod could have a smaller demagnetization factor [24].

$$D_M \propto \frac{d}{l} \quad (5)$$

where d is the diameter of the rod and l is the length. By making the rod longer (in other words, making the path of the magnetic flux longer), the separation between the north pole and the south pole increases, leading to a smaller demagnetizing field. Nevertheless, a very long and thin solenoid may not be the best solution as it occupies too much space because of its length. Besides, a long and thin ferromagnetic rod is brittle and prone to damage. In our preview work [9], a bow-tie shaped core was

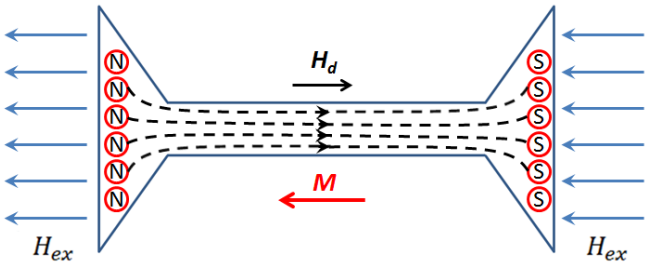

Fig. 5. The demagnetizing field inside a bow-tie-shaped core when applying an external magnetic field

proposed as shown in Fig. 5. By making its two ends broader, the magnetic flux can be more concentrated in the center. Thus the effective permeability in the middle part of the core can be increased. To further improve the performance, a novel helical core is proposed as shown in Fig. 6. Two big circular plates at both ends are used for the flux collection, which could guide more magnetic flux from the air into the ferromagnetic core. In the middle, a helical shaped core is proposed to increase the path of the magnetic flux while the physical length of the core remains unchanged. Therefore, the effective separation between the north pole and south pole is lengthened dramatically which leads to a reduction in the demagnetizing field and an increase in the magnetic flux density.

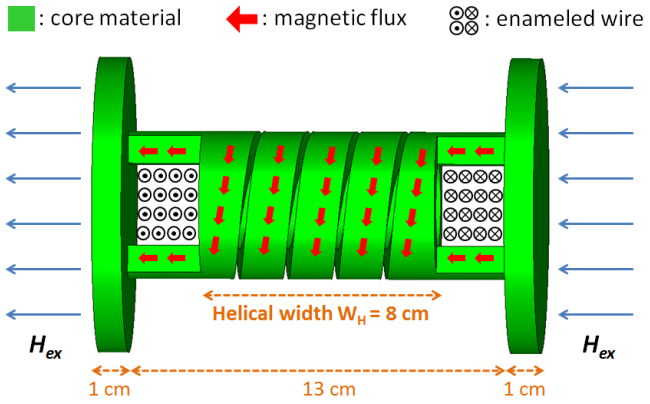

Fig. 6. The helical core proposed

To validate this new design, four different coils depicted in Fig. 7 have been tested in the same uniform magnetic field generated by a Helmholtz coil. All of them have the following configurations for easy comparison:

1. The same physical length of 15 cm;
2. An ideal magnetic core material with the relative permeability μ_r and zero conductivity;
3. 100 turns of enameled wires wound on the core;
4. Placed in the same alternating magnetic field area (7 μT_{rms} at 50 Hz).

The conductivity of the ferromagnetic material is set to zero intentionally to eliminate the eddy current losses, and the hysteresis effect is ignored. Therefore, we can focus on the magnetic properties with different core shapes. CST software is used as the simulation tool and the boundary condition is set to "open" to emulate the free space environment. Fig. 8 shows the simulated magnetic flux density B_{in} inside the four cores when the relative permeability μ_r was assumed to be 10,000. Due to

Copyright (c) 2016 IEEE. Personal use is permitted. For any other purposes, permission must be obtained from the IEEE by emailing pubs-permissions@ieee.org.

This is the author's version of an article that has been published in this journal. Changes were made to this version by the publisher prior to publication.
The final version of record is available at http://dx.doi.org/10.1109/TPEL.2016.2610323

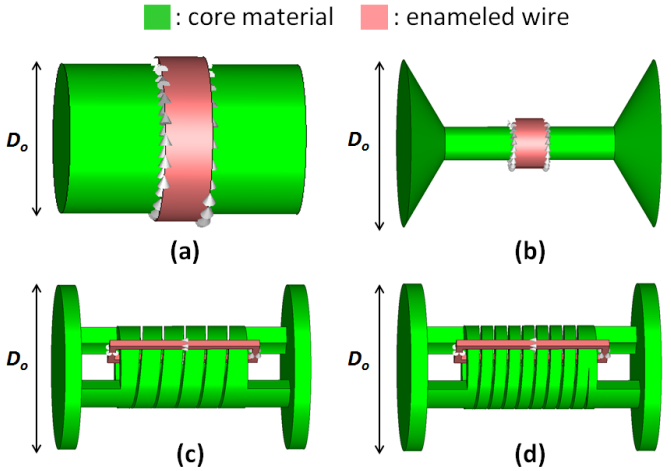

Fig. 7. (a) The conventional solenoid with diameter D_o = 10 cm, (b) the bow-tie coil, (c) the proposed coil with 5 turns of helical slots in the core, and (d) the proposed coil with 10 turns of helical slots in the core

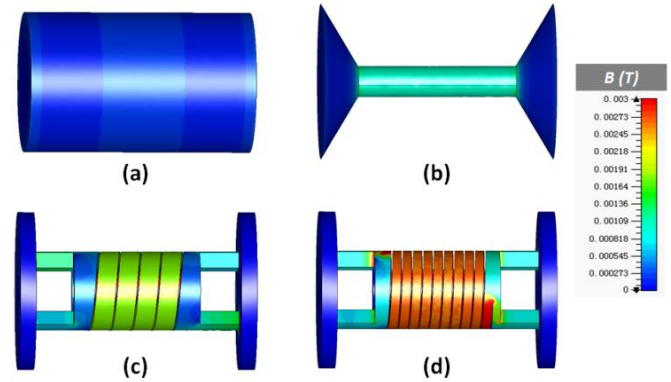

Fig. 8. The simulated magnetic flux density B_{in} inside the four cores (refer to Fig. 7) when the external magnetic density of 7 μT_{rms} is applied and the relative permeability is 10,000

the demagnetization phenomenon, the magnetic flux density was always higher in the center of the core. As clearly depicted in Fig. 8, the flux density in the middle of the rod (0.16 mT_{rms}) and the bow-tie core (1.0 mT_{rms}) was relative small. For the proposed core (c) with 5 turns of helical slots, the flux density in the middle was around 2.0 mT_{rms} which doubles the value of the bow-tie core. When 10 turns of helical slots were introduced to the core as shown in Fig. 8(d), the flux density was enlarged to 3.2 mT_{rms}. This proves that by using the helical core to lengthen the path of the magnetic flux, the demagnetizing field is reduced and the magnetic flux density inside the core is greatly increased. If an enameled wire with a diameter of 0.14 mm is wounded on the four cores for 100 turns, the voltages induced are plotted in Fig. 9 as a function of the relative permeability μ_r. When μ_r is 100,000, the voltage for the helical coil with 11 turns (d), bow-tie coil (b) and solenoid (a) are 69.6 mV, 7.94 mV and 8.98 mV respectively, which indicates that the magnetic flux inside the new helical core can be much larger than the conventional designs. In addition, the four curves become saturated as μ_r increases. For the solenoid (a) and the bow-tie coil (b), their knee points appear when μ_r approaches about 100. In contrast, for helical coil (c), its knee point is around 7000 and the knee point for helical coil (d) is even higher as the voltage still has the tendency to increase when μ_r is larger than 100,000.

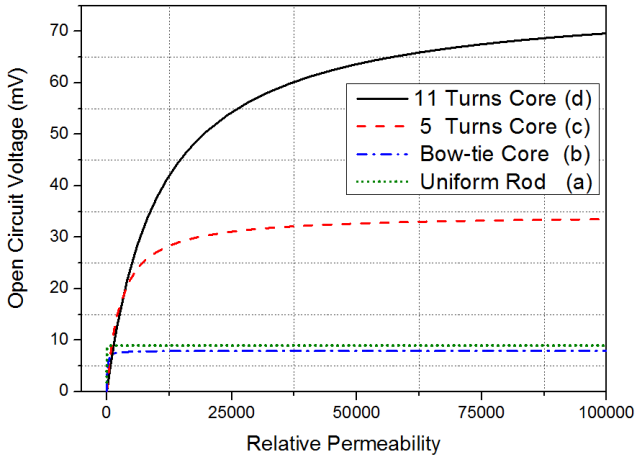

Fig. 9. The simulated open circuit voltage of four coils when the external magnetic density of 7 μT_{rms} is applied

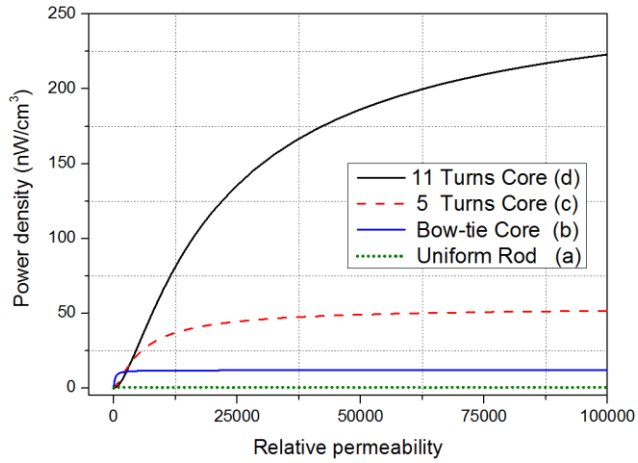

Fig. 10. The calculated power density of four coils when an external magnetic flux density of 7 μT_{rms} is applied

TABLE II
THE PARAMETERS OF THE FOUR CORES WHEN μ_r = 100,000 AND N = 100

Core Type	Solenoid (a)	Bow-tie (b)	Helical (c)	Helical (d)
Open circuit voltage (mV_{rms})	8.98	7.94	33.5	69.6
Path of magnetic flux (cm)	15.0	15.0	47.12	110.7
Wire resistance (Ω)	34.87	6.97	20.0	20.0
Output power (μW)	0.58	2.26	14.1	60.6
Core volume (cm^3)	1178	189	273	273
Power density (nW/cm^3)	0.49	11.9	51.7	223

However, the power density from the coil depends not only on the induced voltage, but also on the coil resistance and the coil volume. If an ideal core material (no loss) is used, the coil resistance is solely determined by the wire resistance. For the 0.14 mm enameled wire, its wire resistivity is 1.11 Ω per meter. Using Equation (2), the coil resistance, the output power and the power densities of the four coils are calculated and concluded in Table II. As depicted in Fig. 10, when μ_r = 100,000, the power density of the helical coil (d) is 223 nW/cm^3

Copyright (c) 2016 IEEE. Personal use is permitted. For any other purposes, permission must be obtained from the IEEE by emailing pubs-permissions@ieee.org.

This is the author's version of an article that has been published in this journal. Changes were made to this version by the publisher prior to publication.
The final version of record is available at http://dx.doi.org/10.1109/TPEL.2016.2610323

which is 20 times higher than that of the Bow-tie coil (b). As a result, the proposed helical core has been demonstrated a much better performance than previous designs due to the longer effective path of the magnetic flux.

C. Core Material Selection

As shown in Fig. 10, the power density of the helical coil increases with the increment of the relative permeability of the core material. However, it is also important to take the core losses into consideration. In general conditions, the core losses can be divided into hysteresis losses and eddy current losses. In this application, as the magnetic field is relatively small and the frequency is only at 50 Hz, the hysteresis losses can be ignored compared to the eddy current losses. Thus, the core losses are mainly determined by eddy current losses. According to [24], the equation to calculate the power consumption of the eddy current losses is:

$$w_{eddy} = \frac{S}{2k\rho}\left(\frac{dB_{in}}{dt}\right)^2 \quad (6)$$

where S is the cross section area in m^2; B_{in} is the magnetic flux density inside the core in T_{rms}; ρ is the material resistivity in Ωm and k is the shape factor. When a helical core is placed inside an alternating magnetic field with a fixed magnitude, the eddy current losses are inversely proportional to the resistivity ρ. As a consequence, the core material should have high relative permeability μ_r as well as high resistivity ρ.

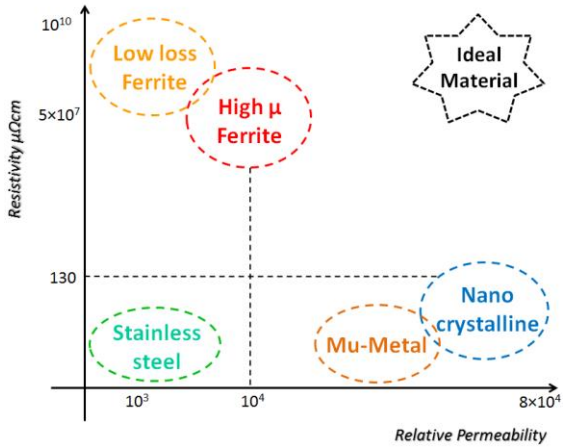

Fig. 11. The relative permeability and resistivity of several typical ferromagnetic materials

Fig. 11 shows the resistivity and relative permeability of some typical ferromagnetic materials [25-28]. Metals and alloys can have very high relative permeability but very low resistivity (usually in the magnitude of a few μΩm [25]). Nanocrystalline usually is considered as a popular ferromagnetic material due to its high relative permeability and reasonably high resistivity among alloys [10-11]. Ferrite is a semiconductor material whose resistivity is extremely high (usually of the order of Ωm). However, its relative permeability is usually lower than 18,000. In this paper, three different materials listed in Table II have been investigated to optimize the power output. The helical coil with 100 winding turns shown in Fig. 8(d) was selected as a testing example. CST was used to calculate the equivalent core resistance and the results are listed in Table III. The nanocrystalline core has the largest core resistance of 87.3 Ω because of the highest permeability and the lowest resistivity. Strong eddy currents were generated inside the core as shown in Fig. 12. Thus, its power output is greatly limited by the eddy current losses, or in other words, the equivalent core resistance. On the other hand, the core resistance of low loss ferrite was tiny (12.1 μΩ) but its power output was still small due to its low relative permeability. For the high μ ferrite core, its core resistance was only 3.97 mΩ which was negligible compared with to the wire resistance 18.3 Ω. Besides, as plotted in Fig. 9(d), the induced voltage becomes saturated when the relative permeability approaches to 15,000. The induced voltage of the nanocrystalline core (66.4 mV) is not significantly bigger than that of high μ ferrite core (40.5 mV). As a result, the high μ ferrite core has the largest power output, which indicates that it is the most suitable material for the proposed helical core.

TABLE III
THE COMPARISON OF THREE DIFFERENT FERROMAGNETIC MATERIALS

Material Type	Low loss Ferrite	High μ Ferrite	Nanocrystal line
Reference	[26]	[27]	[28]
Typical core types	Cylindrical core	Ring core, rod	toroid, 'D' shape
Relative permeability	800	12,000	80,000
Resistivity (μΩm)	10^8	5×10^5	1.3
Induced voltage (mV_{rms})	5.15	40.5	66.4
Core resistance (Ω)	1.21×10^{-5}	3.97×10^{-3}	87.3
Wire resistance (Ω)	18.3	18.3	18.3
Power output (μW)	0.36	22.4	10.4

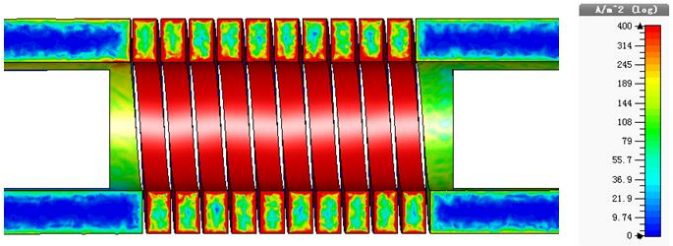

Fig. 12. The simulated eddy current density inside a nanocrystalline core when the external magnetic flux density is 7 μT_{rms}

III. OPTIMIZATION OF THE HELICAL COIL

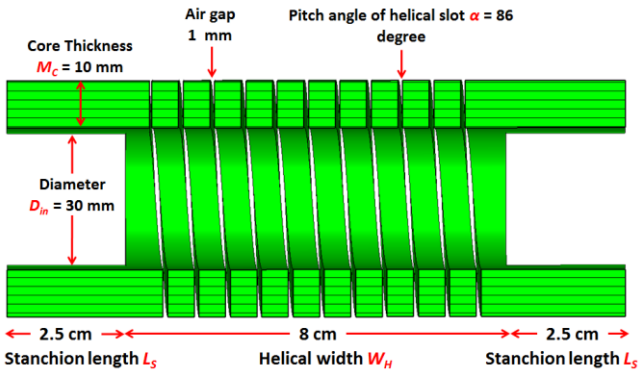

Fig. 13. The cross-section view of a helical core

Copyright (c) 2016 IEEE. Personal use is permitted. For any other purposes, permission must be obtained from the IEEE by emailing pubs-permissions@ieee.org.

This is the author's version of an article that has been published in this journal. Changes were made to this version by the publisher prior to publication.
The final version of record is available at http://dx.doi.org/10.1109/TPEL.2016.2610323

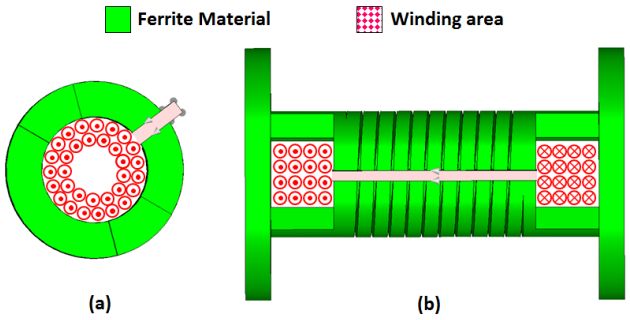

Fig. 14. The winding area of a helical core. (a) the top view, (b) the overall view from outside

As shown in Fig. 8 and Fig. 9, the helical coil with a longer path of the magnetic flux can generate higher voltages. The path of the flux can be made longer by increasing the pitch angle of the helical slot α and the helical width W_H shown in Fig. 13. However, the power output from the harvesting coil also depends on the number of winding turns N and the wire resistance R_{wire}. As shown in Fig. 14, the winding area for a helical core is limited. If the diameter D_{in} and stanchion length L_S are small, there are less winding areas which reduce the power output. Therefore, the shape of the helical core should be optimized to maximize the output power density. The core shown in Fig. 13 is used as a reference and the following three testing conditions are set for the optimizations.

1. The size of two big circular plates as shown in Fig. 6(a) is kept unchanged and the physical length of the entire core is 15 cm long.
2. The high μ ferrite material with μ_r = 12,000 and ρ = 0.5 Ωm is used and the external magnetic flux density is 7 μT_{rms}.
3. An enameled wire with a diameter d of 0.14 mm and the wire resistivity ρ_{wire} of 1.11 Ω per meter is used to wrap on the helical core with the winding area provided.

As the ferrite material is used, the eddy current can be greatly reduced and the overall coil resistance is determined mainly by the wire resistance. To calculate the wire resistance when the core is fully wound, two situations should be considered.

1. When $L_s > 0.5D_{in}$, the wire is fully occupied in the winding area shown in Fig. 14(a). The total layer of the enameled wire K_{total} is:

$$K_{total} = \frac{0.5D_{in}}{d} \tag{7}$$

2. When $L_s < 0.5D_{in}$, the wire is fully occupied in the winding area shown in Fig. 14(b). The total layer K_{total} is:

$$K_{total} = \frac{L_S}{d} \tag{8}$$

Therefore, the total number of turns N inside the helical core can be obtained by:

$$N = \sum_{k=1}^{K_{total}} \left(\frac{\pi}{\arcsin\left(\frac{d}{D_{in} - (2k-1)d} \right)} \right) \tag{9}$$

The wire resistance can be calculated by:

$$R_{wire} = \rho_{wire} \sum_{k=1}^{K_{total}} L_k = \sum_{k=1}^{K_{total}} \left(\frac{\rho_{wire}\pi(2W_H + 2M_c + 8kd)}{\arcsin\left(\frac{d}{D_{in} - (2k-1)d} \right)} \right) \tag{10}$$

where ρ_{wire} is the resistivity of the enameled wire in Ω per meter and M_C is the thickness of the core in m. More detailed derivations and explanations of Equations (7) to (10) can be found in the Appendix.

A. The Pitch Angle α

When the pitch angle of the helical slot becomes bigger and other parameters are unchanged, the path of the magnetic flux increases and the winding area is not affected. It is expected that the power density increases with the increment of the pitch angle as shown in Fig. 15. However, when the pitch angle is too big, the helical core will be very difficult to manufacture and prone to damage especially for the ferrite material.

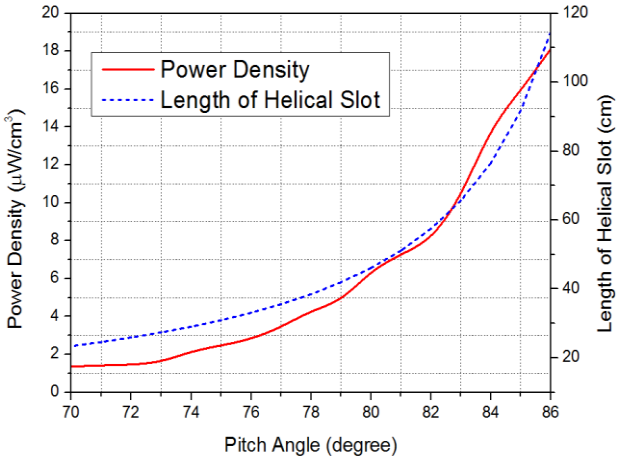

Fig. 15. The simulated power density as a function of the pitch angle

B. Helical Width W_H and Inner Diameter D_{in}

When the pitched angle is fixed, the path of the flux can be made longer by increasing the helical width W_H. However, the stanchion length L_S will decrease as the physical length of the core is limited to 15 cm. This will reduce the winding area shown in Fig. 14(b). As shown in Fig. 16, the magnetic flux generated inside the core increases with the helical width. For the number of turns N, it is constant when the helical width is small as the total layer K_{total} of the enameled wire is determined by the inner diameter D_{in}. When the helical width continues to increase, the stanchion length L_s will be smaller

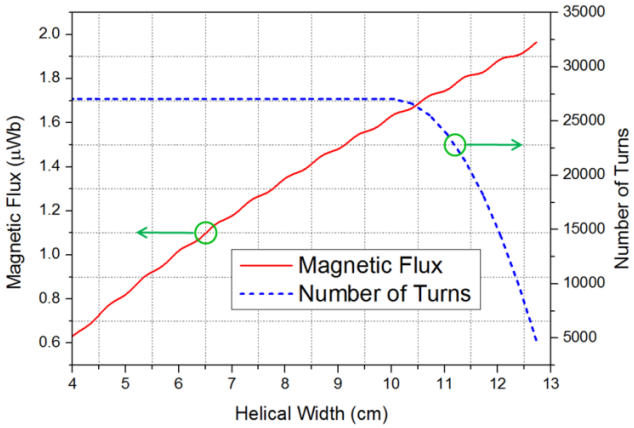

Fig. 16. The simulated magnetic flux and the number of turns as a function of the helical width

Copyright (c) 2016 IEEE. Personal use is permitted. For any other purposes, permission must be obtained from the IEEE by emailing pubs-permissions@ieee.org.

This is the author's version of an article that has been published in this journal. Changes were made to this version by the publisher prior to publication.
The final version of record is available at http://dx.doi.org/10.1109/TPEL.2016.2610323

than the inner radius $D_{in}/2$. In this situation, the layer K_{total} of the wire is proportional to the stanchion length. Thus, the number of turns drops down as the stanchion length decreases. The output power density of the coil is plotted in Fig. 17 as a function of the helical width. The peak value appears when the stanchion length L_s is equal to the inner radius $D_{in}/2$. In this case, both winding areas shown in Fig. 14(a) and (b) are fully utilized.

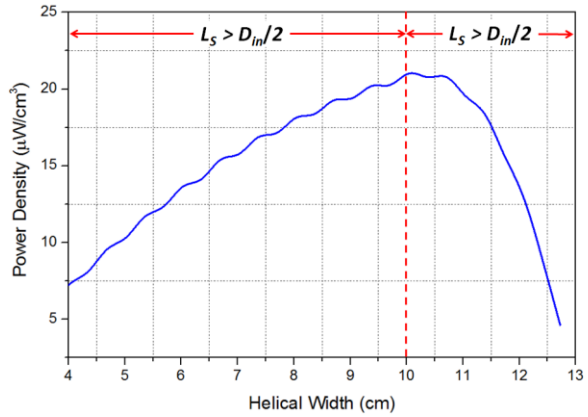

Fig. 17. The simulated power density as a function of the helical width

B. Core Thickness M_C

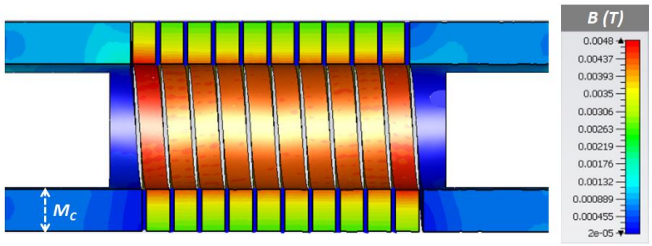

Fig. 18. The magnetic flux density inside a helical core when M_C = 1 cm when the external magnetic flux density is 7 μT_{rms}

By increasing the thickness M_C of the core, more magnetic flux can pass through the core which leads to a higher induced voltage. However, due to the special shape of the helical core, the magnetic flux density inside the core is not uniformly distributed. By applying the magnetic circuit theory, the majority of the magnetic flux tends to travel along the shortest path where the magnetic reluctance is small [24]. As shown in Fig. 18, the magnetic flux density is larger when it is near to the inner edge of the helical core. Therefore, by making the core thicker, the total magnetic flux does not always increase correspondingly. Nevertheless, the wire resistance and core volume are always directly related to the core thickness. As depicted in Fig. 19, when the core thickness is relatively small, the magnetic flux and power density increase with the core thickness M_C. When the thickness is further increased, the magnetic flux becomes saturated and the power density begins to decrease. For the curve of the magnetic flux in Fig. 19, its knee point appears at around 0.8 cm where the helical coil produces the maximum power density.

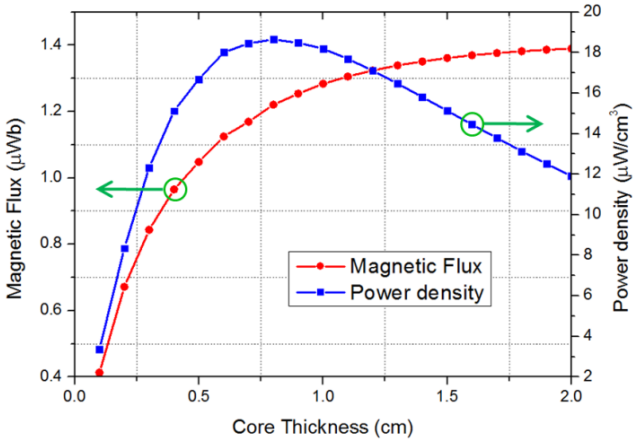

Fig. 19. The simulated magnetic flux and power output as a function of the core thickness

C. Summary

In summary, to increase the power output from the helical coil, the path of the magnetic flux should be made longer and the winding area needs to be fully utilized. The pitch angle of the helical slot should be increased to as big as possible which could significantly boost the power output. When the stanchion length is equal to the inner radius $D_{in}/2$, the winding area inside the helical core can be efficiently used and lead to a high power output. Finally, the core thickness needs to be carefully optimized to achieve higher magnetic flux without making the core too big.

IV. Experimental Validations and Results

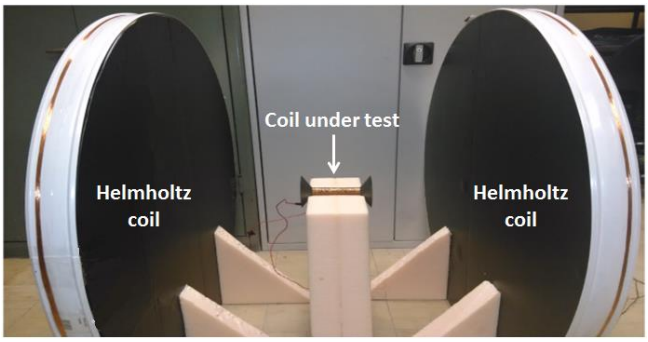

Fig. 20. A Helmholtz coil used to generate a uniform magnetic field in the laboratory

A Helmholtz coil as shown in Fig. 20 (consisting of two identical coil rings) is made to generate a uniform magnetic field to imitate the magnetic field environment near high current equipment. The magnetic flux density can be calculated by [29]:

$$B = (0.8)^{3/2}\frac{\mu_0 NI}{R_H} \quad (11)$$

where μ_0 is the permeability of free space, N is the number of turns wound on the Helmholtz coil; I is the current passing through the coil; R_H is the radius of the Helmholtz coil. In this experiment, the radius of each coil ring is 0.5 meter with 33 turns of conducting wire on it and the two coil rings are separated by half a meter. With a 120 mA_{rms} current passing through the Helmholtz coil, a magnetic flux density of 7 μT_{rms} is generated. Due to the complex shape of the helical core and the physical properties of the ferrite material, it is very difficult and expensive to manufacture the whole core in one ferrite

Copyright (c) 2016 IEEE. Personal use is permitted. For any other purposes, permission must be obtained from the IEEE by emailing pubs-permissions@ieee.org.

This is the author's version of an article that has been published in this journal. Changes were made to this version by the publisher prior to publication.
The final version of record is available at http://dx.doi.org/10.1109/TPEL.2016.2610323

piece. Instead, five pieces shown in Fig. 21 are fabricated separately and then glued together. For each helical piece, a ferrite tube with a suitable size is fabricated and the helical slot is cut carefully by a special grinding tool. The helical core manufactured is shown in Fig. 22. The stanchion length is 1.5 cm and equal to inner radius of the core so that the winding area inside the core can be fully utilized. The pitch angle of the helical slot is 86 degrees. The core would be very fragile and prone to damage if the angle is any higher. High permeability Mn-Zn ferrite [30] is used as the core material with relative permeability 12000 ± 30% and resistivity of 0.15 Ωm.

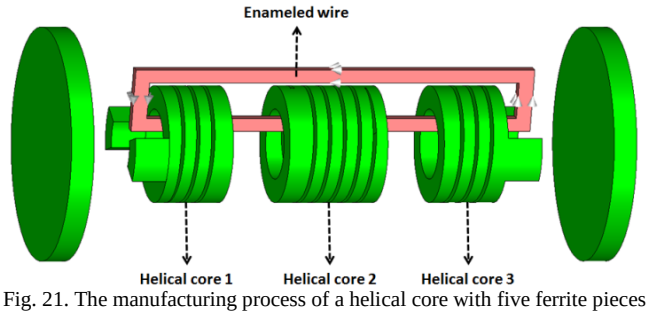

Fig. 21. The manufacturing process of a helical core with five ferrite pieces

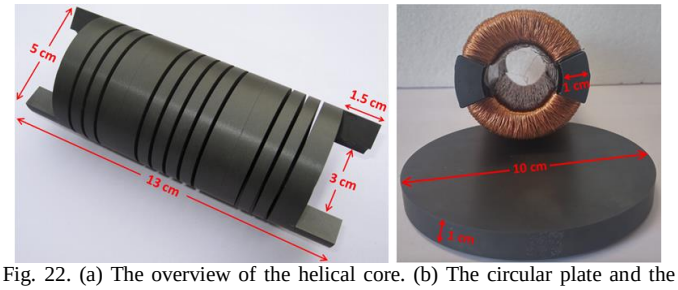

Fig. 22. (a) The overview of the helical core. (b) The circular plate and the helical core with the enameled wire

An enameled wire with a diameter of 0.4 mm and the wire resistivity of 0.136 Ω per meter is used to wind on the helical core. As the core is too long, it is very difficult to find a proper winding machine to wrap the wire on the helical core automatically. Therefore, only 200 and 400 turns of the wire is wound manually just to prove the concept. The coil is put inside the Helmholtz coil and the open circuit voltage is measured using a multimeter. The measured voltage is listed in Table IV and compared to the simulated values. The measured results are slightly lower than the simulated ones which are mainly caused by the fabrication errors of the ferrite core. Firstly, the relative permeability of the ferrite is in the range of 8400 to 15600 according to the datasheet [31], which may bring some uncertainty into the experiment. Secondly, as the whole helical core is made of five separated ferrite pieces, gaps may exist in each contact surface which reduces the overall effective permeability.

TABLE IV
THE MEASURED AND SIMULATED RESULTS OF COIL VOLTAGE

The number of turns	Simulated results (*rms*)	Measured results (*rms*)
N = 200	101.6 mV	91.5 mV
N = 400	203.1 mV	184.7 mV

The effective coil resistance can be measured by a 50 Hz bridge. The power output at the load can be maximized by tuning the compensating capacitor and the load resistance. According to the maximum power transfer theory, the coil resistance should be the same as the load resistance. The wire resistance is measured with a multi-meter and the results are listed in Table V. The measured wire resistance is about 10% higher than the theoretical value as the enameled wire is manually wrapped and cannot be perfectly aligned. This causes a longer wire to achieve the same number of turns and results in the difference between the measured and theoretical values. The overall coil resistance measured at 50 Hz is very close to the wire resistance, proving that the eddy current losses are minimized by using the ferrite material.

TABLE V
THE MEASURED AND CALCULATED RESULTS OF THE COIL RESISTANCE

Number of turns	R-wire (theory)	R-wire (measured)	R-coil (measured)
N = 200	6. 11 Ω	6.85 Ω	6.88 Ω
N = 400	12.54 Ω	13.88 Ω	13.96 Ω

TABLE VI
THE MEASURED AND CALCULATED RESULTS OF THE POWER OUTPUT

The number of turns	Simulated results	Measured results
N = 200	0.42 mW	0.31 mW
N = 400	0.83 mW	0.61 mW
N = 2000	3.96 mW	2.86 mW (predicted)

The helical coil with 400 turns can deliver a power output of 0.61 mW under the magnetic flux density of 7 μT_{rms}. When more windings are added on the core, more power output from the coil can be achieved [9]. From Equation (9) and in the ideal case, the fabricated core shown in Fig. 22 can wrap a maximum of 3310 turns of enameled wire (diameter d = 0.4 mm). However, due to the imperfect winding (e.g. wire misalignments), we conservatively estimate that only 2000 turns of wire can be wound on the core. In this case, it can be predicted that the coil voltage will increase to 910 mV as the induced voltage is linearly proportional to the number of turns. According to Equations (9) and (10), when N = 2000, the wire resistance would be 66 Ω. As a consequence, the predicted power output from the core is 2.86 mW when N = 2000.

V. DISCUSSIONS AND PERFORMANCE COMPARISON

The measured power density for the helical coil with 400 turns is 2.1 $\mu W/cm^3$ at 7 μT_{rms}. If the number of turns can be increased to 2000, the predicted power output will be 7.9 $\mu W/cm^3$. Both values are lower than the simulated results (21 $\mu W/cm^3$ at 7 μT_{rms}) shown in Fig. 17. This is mainly limited by the ferrite core fabrication and low number of winding turns. If a specific injection mold can be made available, a helical core can be manufactured in one ferrite piece and more helical slots can be cut compared to the fabricated core shown in Fig. 22(a). Therefore, the measured output power can be increased. Furthermore, by using a mold, the fabrication process can be

Copyright (c) 2016 IEEE. Personal use is permitted. For any other purposes, permission must be obtained from the IEEE by emailing pubs-permissions@ieee.org.

This is the author's version of an article that has been published in this journal. Changes were made to this version by the publisher prior to publication.
The final version of record is available at http://dx.doi.org/10.1109/TPEL.2016.2610323

simplified and the unit price of a helical core can be reduced dramatically. If a proper coil winding machine can be found and utilized, more wires can be efficiently wounded on the core which also leads to a higher power output. Despite of these limitations, the measured power density is still better than previous reported designs as demonstrated in Table VII. The power density in [15] is small as they used the cast iron as the core material, which suffered greatly from the eddy current losses. If more wires can be wound on this helical core, the power density will increase as shown in Fig. 23. When N = 2000, its predicted power density (9.8 μW/cm^3) is 4 times larger than that of the bow-tie coil [9] which was achieved with 40,000 turns of wires.

TABLE VII
THE COMPARISON OF DIFFERENT DESIGNS

The coil type	Bow-tie coil [9]	Solenoid [15]	Helical coil N = 400
Physical length	15 cm	50 cm	15 cm
Applied flux density	7 μT$_{rms}$	18.5 μT$_{rms}$	7 μT$_{rms}$
The number of turns	40,000	40,000	400
The wire diameter	0.14 mm	Unknown	0.4 mm
Induced voltage	2.95 V$_{rms}$	10. 5 V$_{rms}$	185 mV$_{rms}$
Coil resistance	6.03 kΩ	33 kΩ	13.96 Ω
Volume	188 cm^3	981 cm^3	292 cm^3
Power output	360 μW	833 μW	612 μW
Power density	1.86 μW/cm^3	0.85 μW/cm^3	2.10 μW/cm^3

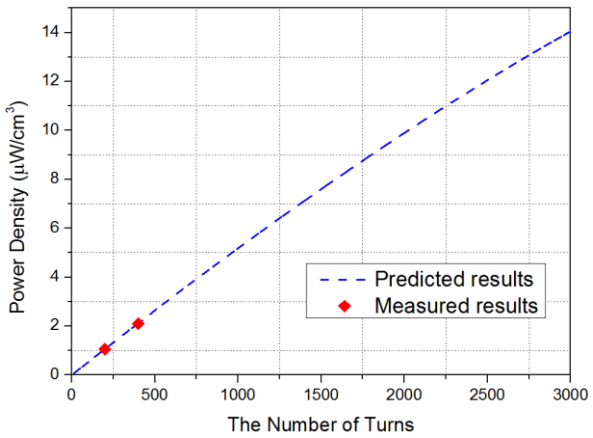

Fig. 23. The predicted power output as a function of the number of turns

From the experiment, 612 μW was collected at the load by using the helical coil with 400 turns, which might be enough to power a small wireless sensor [31]. The power harvested can be further increased to 2.86 mW if the coil can have 2000 turns of wires. The power consumption of a GPRS data logger is 3.6 W [32]. If the data is collected every 30 minutes and the data logger takes a maximum of 1 minute to transmit the information to the server, the average power consumption would be 120 mW. As a result, a larger helical core shown in Fig. 24 can be designed to collect more power.

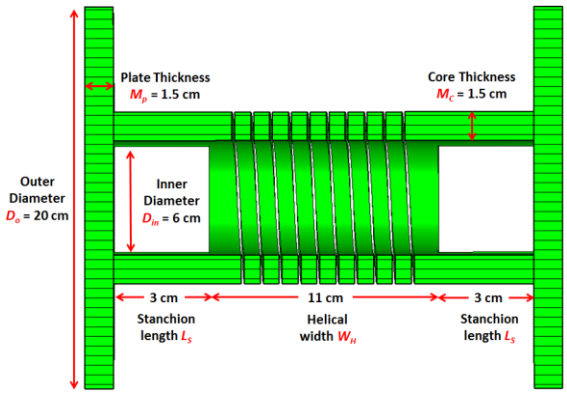

Fig. 24. The cross section view of a larger and longer helical core

The physical length of the core is increased to 25 cm so that the path of the magnetic flux can be further lengthened. Meanwhile, the outer diameter D_o of the big circular plate is enlarged to guide more flux passing through the helical core. As the inner diameter D_{in} is increased to 6 cm, we assume that around 8,000 turns of enameled wires with the diameter of 0.4 mm can be wound on the core. If this coil can be placed slightly closer to power equipment where the magnetic flux density is higher than 11 μT$_{rms}$, more than 160.5 mW can be harvested. This means that the large helical coil shown in Fig. 24 is able to power a GPRS data logger when it is near any equipment carrying sufficient currents.

VI. CONCLUSIONS

In this paper, a completely new design of a special coil has been proposed to scavenge the magnetic field energy near high power equipment such as overhead lines, transformers, switchgears, etc. The coil does not need to be clamped to the power cable but can be installed almost anywhere in a substation or under overhead lines. It is highly efficient thus a range of sensors can be powered. This is not always possible for the cable-clamped energy harvester.

A novel helical core has been proposed and optimized to produce a much higher power density compared to conventional designs. This was based on theoretical analysis and subsequently verified by experimental measurements. The special design of the helical shape has dramatically lengthened the path of the magnetic flux, which reduced the demagnetization and led to a higher power output. The core material was selected by compromising high permeability and low eddy current losses. High permeability ferrite was identified as the most suitable core material, given its high relative permeability and ultra-low conductivity. The geometry shape of the helical core has been optimized to increase the path of the magnetic flux and better utilize the winding area available inside the core. From the experimental results, the power density of a helical coil with only 400 turns was already greater than a recently reported result if both coils were placed into the same magnetic field. If the fabricated coil has 2000 turns of wire, its predicted power density (9.8 μW/cm^3) is 4 times larger than previous designs. Thus, the proposed solution is extremely efficient on harvesting the magnetic field energy near high current equipment and can be used to power a range of wireless sensors.

Copyright (c) 2016 IEEE. Personal use is permitted. For any other purposes, permission must be obtained from the IEEE by emailing pubs-permissions@ieee.org.

This is the author's version of an article that has been published in this journal. Changes were made to this version by the publisher prior to publication.
The final version of record is available at http://dx.doi.org/10.1109/TPEL.2016.2610323

APPENDIX

To calculate the wire resistance, it is critical to figure out how many layers of the enameled wire are wound inside the helical core. The parameter K_{total} is defined to express the total layer of the enameled wire existing inside a helical core. Some examples are provided in Fig. 25 to help better understand the definition of K_{total}.

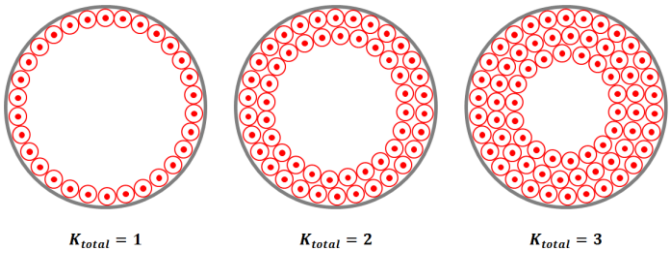

Fig. 25. The definition of the total layer of the enameled wire inside a core

For a particular layer of the wire inside a helical core, the number of turns in this layer N_k can be correlated to the wedge angle α shown in Fig. 26.

$$\alpha = \frac{2\pi}{N_k} \tag{12}$$

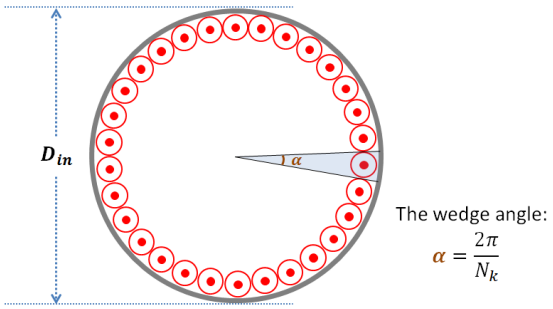

Fig. 26. The wedge angle α defined inside a helical core

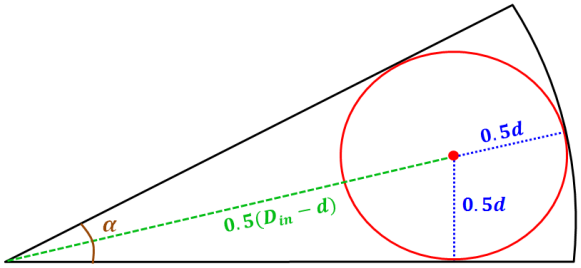

Fig. 27. The parameters of a small wedge

The wedge angle α can be obtained by:

$$\alpha = 2\arcsin\left(\frac{d}{D_{in} - d}\right) \tag{13}$$

where d is the diameter of the enameled wire and D_{in} is the inner diameter of helical core shown in Fig. 13. By combining Equation (12) and (13), the number of turns in this particular layer N_k can be derived:

$$N_k = \frac{\pi}{\arcsin\left(\frac{d}{D_{in} - d}\right)} \tag{14}$$

Assuming that there are K_{total} layers of enameled wire inside the core, the total number of turns N_{total} can be calculated by the summation of the number of turns in each layer N_k.

$$N_{total} = \sum_{k=1}^{K_{total}} N_k = \sum_{k=1}^{K_{total}} \left(\frac{\pi}{\arcsin\left(\frac{d}{D_{in} - (2k-1)d}\right)}\right) \tag{15}$$

The length of the enameled wire at the k^{th} layer L_k can be expressed by:

$$L_k = N_k(2W_H + 2M_c + 8kd) \tag{16}$$

where W_H is the helical width and M_c is the core thickness shown in Fig. 13. The total length of all the enameled wire L_{total} inside the core can be obtained by the summation of L_k in each layer

$$L_{total} = \sum_{k=1}^{K_{total}} L_k = \sum_{k=1}^{K_{total}} (N_k(2W_H + 2M_c + 8kd)) \tag{17}$$

By combining Equation (15) and (17), the wireless resistance R_{wire} can be calculated:

$$R_{wire} = \rho_{wire} \sum_{k=1}^{K_{total}} L_k = \sum_{k=1}^{K_{total}} \left(\frac{\rho_{wire}\pi(2W_H + 2M_c + 8kd)}{\arcsin\left(\frac{d}{D_{in} - (2k-1)d}\right)}\right) \tag{18}$$

where ρ_{wire} is the resistivity of the enameled wire in Ω per meter.

REFERENCES

[1] D. Hostick, D. Belzer and S. Hadley, "Projecting Electricity Demand in 2050", Pacific Northwest National Laboratory, Washington, 2014
[2] D. J. Spoor and J. P. Roberts, "Development and Experimental Validation of a Weather-Based Dynamic Line Rating System", *Innovative Smart Grid Technologies Aisa (ISGT)*, 2011, pp. 1-7
[3] Y. Biçen; F. Aras and Y. Kirkrici, "Lifetime Estimation and Monitoring of Power Transformer Considering Annual Load Factors", *IEEE Transaction on Dielectrics and Electrical Insulation*, Vol. 21, Issue. 3, 2014, pp. 1360-1367
[4] D. M. Green, J. P. Gentle and K. S. Myers, "A Comparison of Real-Time Thermal Rating Systems in the U.S. and the U.K.", *IEEE Transactions on Power Delivery*, Vol. 29, Issue: 4, 2014, pp. 1849-1858
[5] Z. Wang, M. Begovi, and J. Wang, "Analysis of Conservation Voltage Reduction Effects Based on Multistage SVR and Stochastic Process", *IEEE Transactions on Smart Grid*, Vol. 5, No. 1, 2014, pp. 431-439
[6] I. E. Portugu és, P. J. Moore, I. A. Glover, C. Johnstone and R.H. Mckosky, "RF-Based Partial Discharge Early Warning System for Air-Insulated Substations", *IEEE Transactions on Power Delivery*, Vol. 24, No. 1, 2009, pp. 20-29
[7] V. C. Gungor, B. Lu, G. P. Hancke, "Opportunities and Challenges of Wireless Sensor Networks in Smart Grid", *IEEE Transaction on Industrial Electronics*, Vol. 57, NO. 10, 2010, pp. 3557 – 3564
[8] V. Raghunathan, A. Kansal, J. Hsu, J. Friedman, Mani Srivastava, "Design considerations for solar energy harvesting wireless embedded systems," *Information Processing in Sensor Networks*, 2005, pp. 457-462
[9] S. Yuan, Y. Huang, J. Zhou, Q. Xu and C. Song, "Magnetic Field Energy Harvesting Under Overhead Power Lines", *IEEE Transaction on Power Electronics*, Vol. 30, Issue 11, 2015, pp. 6191 – 6202
[10] J. Moon, S.B. Leeb, "Analysis Model for Magnetic Energy Harvesters", *IEEE Transactions of Power Electronics*, Vol.30, Issue: 8, 2015, pp. 4302-4311
[11] J. Moon, S.B. Leeb, "Power Electronic Circuits for Magnetic Energy Harvesters", *IEEE Transactions on Power Electronics*, Vol.31, Issue: 1, 2016, pp. 270-279
[12] T. Hosseinimehr and A. Tabesh, "Magnetic Field Energy Harvesting from AC Lines for Powering Wireless Sensor Nodes in Smart Grids", *IEEE Transactions on Industrial Electronics*, pp. 1-1, 2016.
[13] J. Moon and S. Leeb, "Power loss analysis with high primary current in magnetic energy harvesters", *2015 IEEE 16th Workshop on Control and Modeling for Power Electronics (COMPEL)*, 2015.
[14] M. J. Moser, T. Bretterklieber, H. Zangl and G. Brasseur, "Strong and Weak Electric Field Interfering: Capacitive Icing Detection and

Copyright (c) 2016 IEEE. Personal use is permitted. For any other purposes, permission must be obtained from the IEEE by emailing pubs-permissions@ieee.org.

This is the author's version of an article that has been published in this journal. Changes were made to this version by the publisher prior to publication.
The final version of record is available at http://dx.doi.org/10.1109/TPEL.2016.2610323

Capacitive Energy Harvesting on a 220-kV High-Voltage Overhead Power Line", *IEEE Transaction on Industrial Electronics*, Vol. 58, No. 7, 2011, pp. 2597-2604
[15] N. M. Roscoe and M. D. Judd, "Harvesting Energy from Magnetic Fields to Power Condition Monitoring Sensors", *IEEE Sensors Journal*, Vol. 13, Issue: 6, 2013, pp. 2263-2270
[16] K. Tashiro, H. Wakiwaka, S. Inoue, and Y. Uchiyama, "Energy Harvesting of Magnetic Power-Line Noise", *IEEE Transactions on Magnetics*, Vol. 47, Issue: 10, 2011, pp. 4441-4444
[17] N. Roscoe and M. Judd, "Optimization of Voltage Doublers for Energy Harvesting Applications", *IEEE Sensors Journal*, vol. 13, no. 12, pp. 4904-4911, 2013.
[18] R. Moghe, Yi Yang, F. Lambert and D. Divan, "A scoping study of electric and magnetic field energy harvesting for wireless sensor networks in power system applications", *2009 IEEE Energy Conversion Congress and Exposition*, 2009.
[19] R. Moghe, F. Lambert and D. Divan, "Smart Stick on Sensors for the Smart Grid", *IEEE Trans. Smart Grid*, vol. 3, no. 1, pp. 241-252, 2012.
[20] National Grid, "On-line calculator | EMFs.info", *EMFs.info*, http://www.emfs.info/sources/overhead/ohl-calculating/calculator/, 2016
[21] I. Said, H. Hussain and V. Dave, "Characterization of magnetic field at distribution substations", *2010 9th International Conference on Environment and Electrical Engineering*, 2010.
[22] K. Choma and M. Etezadi-Amoli, "Magnetic field measurements in a 345 kV substation", *2011 North American Power Symposium*, 2011.
[23] A. Safigianni and C. Tsompanidou, "Electric- and Magnetic-Field Measurements in an Outdoor Electric Power Substation", *IEEE Transactions on Power Delivery*, vol. 24, no. 1, pp. 38-42, 2009.
[24] D. Jiles, "Introduction to Magnetism and Magnetics Materials", in *Magnetism*, 2nd ed. Ames, Iowa: Chapman & Hall, 1998, pp. 49-51
[25] C. Heck, "Magnetic Materials and their Applications", London Butterworths, pp. 212-213, 1974
[26] Ferroxcube, 3R1 Material Specification, datasheet available at http://www.ferroxcube.com/FerroxcubeCorporateReception/datasheet/3r1.pdf, 2008
[27] Ferroxcube, 3E12 Material Specification, datasheet available at http://www.ferroxcube.com/FerroxcubeCorporateReception/datasheet/3e12.pdf, 2013
[28] Wiltan, Nanocrystalline Toroidal Cores, datasheet available at http://media.wix.com/ugd/aba60c_dae514a99bb04303b0630f221483c0dc.pdf, 2013
[29] E. Javor and T. Anderson, "Design of a Helmholtz coil for low frequency magnetic field susceptibility testing", *1998 IEEE EMC Symposium. International Symposium on Electromagnetic Compatibility. Symposium Record (Cat. No.98CH36253)*.
[30] Mn-Zn ferrite, R12k Material Characteristics, datasheet available at www.chinadmegc.com/material_download.php?22, 2014
[31] Memsic, Wireless Measurement System (MPR2400VB), http://www.memsic.com/userfiles/files/Datasheets/WSN/6020-0060-04-B_MICAz.pdf, 2013
[32] Invisible-systems, Technical Datasheet: Gateway GPRS, GPS & RF, http://www.invisible-systems.com/solutions/pdf/Gateway%20GPRS%20GPS%20RF.pdf, 2015

Sheng Yuan received B.Eng degree (first class) in microelectronics and telecommunication engineering from the University of Liverpool, UK in 2012 and received the PhD degree in electrical engineering & electronics from the University of Liverpool, UK, in 2016.

He is now with the Department of Intelligent Transportation System, Arup Group Limited, Newcastle, UK. His research interests include wireless energy harvesting, ferromagnetic material, indoor navigation system, energy management circuit, wireless power transfer, RFID and intelligent transportation system.

Yi Huang (S'91–M'96–SM'06) received B.Sc. degree in physics from Wuhan University, China, the M.Sc. (Eng.) degree in microwave engineering from NRIET, Nanjing, China, and the D.Phil. degree in communications from the University of Oxford, Oxford, U.K., in 1994.

He has been conducting research in the areas of wireless communications, applied electromagnetics, radar and antennas for the past 25 years. His experience includes 3 years spent with NRIET (China) as a Radar Engineer and various periods with the Universities of Birmingham, Oxford, and Essex, in the U.K., as a member of research staff. He worked as a Research Fellow at British Telecom Labs in 1994, and then joined the Department of Electrical Engineering & Electronics, the University of Liverpool, U.K., as a Faculty member in 1995, where he is now a Full Professor in Wireless Engineering, the Head of High Frequency Engineering Research Group, and M.Sc. Programme Director. He has published over 200 refereed papers in leading international journals and conference proceedings, and is the principal author of the popular book Antennas: from Theory to Practice (Wiley, 2008). He has received many research grants from research councils, government agencies, charity, EU, and industry, acted as a consultant to various companies, and served on a number of national and international technical committees.

Prof. Huang has been an Editor, Associate Editor, or Guest Editor of four of international journals. He has been a keynote/invited speaker and organiser of many conferences and workshops (e.g., IEEE iWAT 2010, WiCom 2006, 2010, and LAPC2012). He is at present the Editor-in-Chief of Wireless Engineering and Technology, a UK National Rep of European COST-IC1102, an Executive Committee Member of the *IET Electromagnetics PN*, and a Fellow of IET, U.K

Jiafeng Zhou received a BSc degree in Radio Physics from Nanjing University, Nanjing, China, in 1997, and a Ph.D. degree from the University of Birmingham, Birmingham, U.K., in 2004. His doctoral research concerned high-temperature superconductor microwave filters.

From July 1997, for two and a half years he was with the National Meteorological Satellite Centre of China, Beijing, China. From August 2004 to April 2006, he was with the University of Birmingham, where his research concerned phased arrays for reflector observing systems. Then he moved to the Department of Electronic and Electrical Engineering, University of Bristol, Bristol, U.K until August 2013. His research in Bristol was on the development of highly efficient and linear amplifiers. He is now with the Department of Electrical Engineering and Electronics, University of Liverpool, Liverpool, UK. His past and current research interests include microwave power amplifiers, filters, electromagnetic compatibility, energy harvesting and wireless power transfer.

Qian Xu received the B.Eng. and M.Eng. degrees from the Department of Electronics and Information, Northwestern Polytechnical University, Xi'an, China, in 2007 and 2010, and received the PhD degree in electrical engineering from the University of Liverpool, U.K, in 2016.

He worked as a RF engineer in Nanjing, China in 2011 and an Application Engineer in CST, Shanghai, China in 2012. His research interests include statistical electromagnetics, computational electromagnetics, reverberation chamber and anechoic chamber.

Copyright (c) 2016 IEEE. Personal use is permitted. For any other purposes, permission must be obtained from the IEEE by emailing pubs-permissions@ieee.org.

This is the author's version of an article that has been published in this journal. Changes were made to this version by the publisher prior to publication.
The final version of record is available at http://dx.doi.org/10.1109/TPEL.2016.2610323

Chaoyun Song was born in Gansu, China, in 1990. He received the B.Eng degree (Hons) in telecommunication engineering from Xi'an Jiao Tong Liverpool University, Suzhou, China, in 2012 and the M.Sc. degree with distinction in microelectronics and telecommunication from the University of Liverpool, Liverpool, United Kingdom, in 2013. He is currently working toward the Ph.D. degree at the University of Liverpool, Liverpool, UK.

His research interests include antenna design, power management circuit, wireless power transfer and energy harvesting, and wearable antennas

Guoqiang Yuan received the B.Eng degree (first class) in Applied Physics from Chongqing University, Chongqing, China, in 1986 and he received the M.Sc. (Eng.) in laser crystal material at Chinese Academy of Sciences, Shanghai, China, in 1989.

He is now the director of Shanghai CSY Ltd, a dynamic and innovative company that designs and manufactures a wide range of sensors, ferrite products and plastic parts. His research interests include laser crystal material, ferromagnetic material, ceramic material, inorganic material, microelectronic packaging technology and automotive sensors.

Copyright (c) 2016 IEEE. Personal use is permitted. For any other purposes, permission must be obtained from the IEEE by emailing pubs-permissions@ieee.org.